Available online at www.sciencedirect.com
SCIENCE DIRECT
Journal of Solid State Chemistry 179 (2006) 1029–1034
JOURNAL OF SOLID STATE CHEMISTRY
www.elsevier.com/locate/jssc

Low-temperature synthesis and structure characterization of the serials $Y_{2-\delta}Bi_{\delta}Sn_2O_7$ ($\delta = 0-2.0$) nanocrystals

KunWei Li, TingTing Zhang, Hao Wang*, Hui Yan

The College of Materials Science and Engineering, Beijing University of Technology, Beijing 100022, China

Received 7 September 2005; received in revised form 26 October 2005; accepted 9 December 2005
Available online 30 January 2006

Abstract

A series of $Y_{2-\delta}Bi_{\delta}Sn_2O_7$ ($\delta = 0$, 0.1, 0.3, 0.5, 1.0, 1.5, and 2.0) nanocrystals were successfully synthesized by the low-temperature hydrothermal method. The structures of serial compounds were characterized by X-ray diffraction (XRD) and infrared (IR) absorption spectroscopy, and were further refined by TOPAS software by Bruker AXS using the whole powder pattern data. These materials form a series of cubic pyrochlore-type oxides at low temperature and are consistent with Vegards' law, indicating that the hydrothermal synthesis conferred a higher chemical homogeneity and reactivity on the powders, and resulting in low crystallization temperature for the pyrochlore-phase complex oxides.

Keywords: Hydrothermal method; Nanocrystal; Yttrium stannate; Bismuth stannate; Pyrochlore

1. Introduction

The series of rare-earth pyrochlore $Y_{2-\delta}Bi_{\delta}Sn_2O_7$ ($\delta = 0-2.0$) are of considerable importance for numerous applications including piezoelectricity, dielectric, resistance to radiation damage, and have been specially investigated as heterogeneous catalysts for a variety of processes [1–5]. The extensive application of these complex oxides may be partially understood as being related to the chemical activity of the $6s^2$ lone pair electrons of Bi (III), the high-temperature stability of pyrochlore, and the morphologies and sizes of particles which in turn largely depend on the preparation methods and preparation conditions. In general, phase-pure, crystalline, nanosized $Y_{2-\delta}Bi_{\delta}Sn_2O_7$ with a narrow size distribution is highly desirable to serve most of their intended purposes, especially in the catalysts and rapidly developing nanoelectronic and nanooptoelectronic devices.

Great efforts have been made to devise versatile techniques such as high-temperature solid-state reaction [6], co-precipitation [7], sol–gel [8] and so forth, to synthesize pyrochlore $Y_{2-\delta}Bi_{\delta}Sn_2O_7$. However, the above conventional methods for the preparation of complex pyrochlore oxides are troublesome as they all employ a relatively high temperature (ca. 1000 °C) for a very long time. Moreover, as well known, the high-temperature solid-state reaction method can easily lead to local chemical heterogeneity and large-sized particles, which may result in multiphase powders [9]. Ismunandar et al. [10] have investigated the structural properties of serials Y-doped $Bi_2Sn_2O_7$ prepared by solid-state reaction. They found that the materials form two series of solid solutions with $\delta > 1$ and < 1, and a discontinuity in the lattice parameter versus composition plot near $\delta = 1$.

Soft chemical methods have offered an alternative to produce smaller-sized, chemically homogeneous particles [11]. The use of solution-based soft chemical methods to prepare nanocrystalline materials is expected to result in chemically homogeneous and phase-pure specimens, a narrow particles size distribution, and low crystallization temperatures of the materials. In this paper, we have firstly introduced the soft chemical method for the synthesis of a series of $Y_{2-\delta}Bi_{\delta}Sn_2O_7$ ($\delta = 0$, 0.1, 0.3, 0.5, 1.0, 1.5, and 2.0) nanocrystals by a low-temperature (200 °C) hydrothermal technique.

*Corresponding author. Fax: +86 10 67392412.
E-mail address: haowang@bjut.edu.cn (H. Wang).

0022-4596/$ - see front matter © 2005 Elsevier Inc. All rights reserved.
doi:10.1016/j.jssc.2005.12.026

2. Experimental

2.1. Synthesis

The starting reagents were analytical-grade yttrium nitrate hydrate, $Y(NO_3)_3 \cdot 6H_2O$, bismuth nitrate hydrate, $Bi(NO_3)_3 \cdot 6H_2O$, and tin chloride hydrate, $SnCl_4 \cdot 5H_2O$. The exact quantity of Y, Bi and Sn in the nitrate hydrate and chloride hydrate was determined by thermogravimetric analysis. An amount of $Y(NO_3)_3 \cdot 6H_2O$, $Bi(NO_3)_3 \cdot 6H_2O$ and $SnCl_4 \cdot 5H_2O$ were dissolved in deionized water, respectively. And then, the solutions were mixed in the appropriate molar ratios ($\delta = 0$, 0.1, 0.3, 0.5, 1.0, 1.5, and 2.0 in $Y_{2-\delta}Bi_\delta Sn_2O_7$) while stirring vigorously on a magnetic stirrer. Then some amount of NaOH solution was dropped to the above solution to form white precipitation mixtures with nominal NaOH concentrations of 1.0 M. The mixture was stirred at ambient temperature for 10 min and then sealed in a 50-ml stainless autoclave Teflon lined and allowed to heat at 200 °C for 12 h under autogenous pressure. After natural cooling, the products were filtered off, washed with deionized water, and dried at 110 °C.

2.2. Characterization

X-ray powder diffraction (XRD) data were obtained using a Bruker Advanced D8 powder diffractometer equipped with a focusing Ge (1 1 1) incident beam monochromator (Cu$K\alpha_1$ radiation, $\lambda = 1.5406$ Å). Finely ground samples were placed on a zero-background quartz sample holder. Intensity data were collected at ambient temperature in the 2θ range between 20° and 70° with a step width of 0.02° and a 2 s count time. Phases present were identified by comparison with the PDF2 database. The structure refinements were undertaken with TOPAS software by Bruker AXS using the whole powder pattern data. From the refinements, lattice parameters for each sample were obtained with an accuracy of ± 0.001 Å. Fourier transform infrared (FTIR) spectra were recorded on a Bruker Vector-22 spectrometer in the transmission mode (KBr method). Transmission electron microscopy (TEM) and selected area electron diffraction (SAED) were taken on a JEOL-JEM 2010F transmission electron microscope, using an accelerating voltage of 210 kV.

3. Results and discussion

The preparation conditions of samples $Y_{2-\delta}Bi_\delta Sn_2O_7$ ($\delta = 0$, 0.1, 0.3, 0.5, 1.0, 1.5, and 2.0) synthesized by hydrothermal method are similar. So we take $Y_{2-\delta}Bi_\delta Sn_2O_7$ ($\delta = 0$ and 2.0) as the example to illustrate the others. The XRD patterns of the samples $Y_{2-\delta}Bi_\delta Sn_2O_7$ synthesized under different NaOH concentrations (0, 1, and 3 mol/L) are shown in Fig. 1a ($\delta = 0$) and b ($\delta = 2.0$), respectively. In Fig. 1a, by comparing with the PDF2 database, we noted that three kinds of materials were formed at different NaOH concentrations. When the NaOH concentration was 0 mol/L, the product was cassiterite SnO_2 with tetragonal system (JCPDS 411445), while the NaOH concentration was 3 mol/L the product was ascribed to yttrium hydroxide, $Y(OH)_3$, with the hexagonal system (JCPDS 832042). Only when the concentration of NaOH was 1 mol/L, the diffraction lines can be readily indexed to a pure cubic-phase $Y_2Sn_2O_7$ with pyrochlore structure conforming to the *Fd*3*m* space group (JCPDS 201418). The widening behavior of the diffraction peaks of the sample indicates that the sizes are very small, according to the well-known Debye–Scherrer formula.

In Fig. 1b, we found that when the NaOH concentration was 0 mol/L, the product was bismoclite, BiOCl, with tetragonal system (JCPDS 06-0249). When the NaOH concentration was 1 mol/L, the product was $Bi_2Sn_2O_7$ (JCPDS 17-0457). When the concentration of NaOH was increased to 3 mol/L, the sample was the mixture of $Bi_2Sn_2O_7$ (JCPDS 17-0457) and $Bi_2O_{2.33}$ (JCPDS 27-0051).

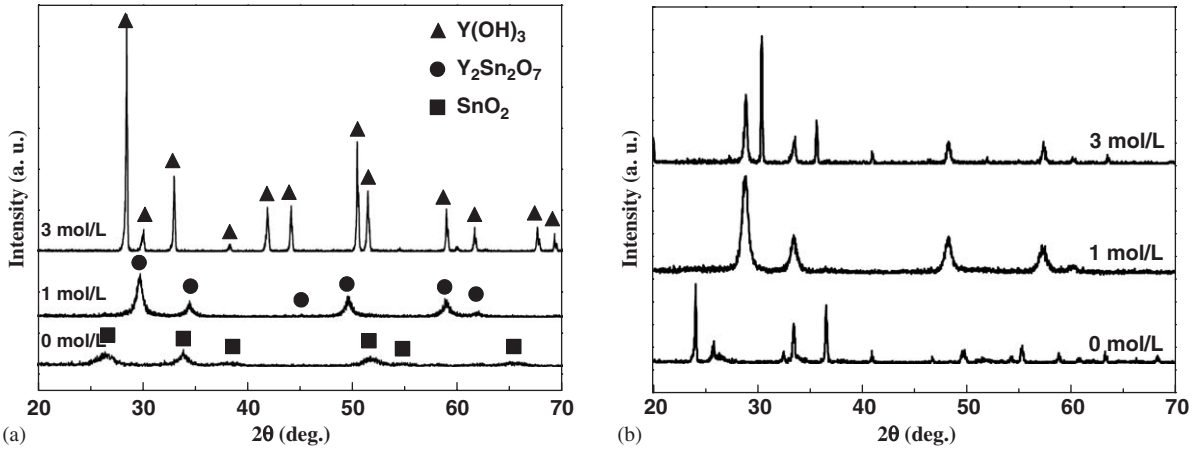

Fig. 1. The XRD for the samples $Y_{2-\delta}Bi_\delta Sn_2O_7$ synthesized under different NaOH concentrations (0, 1 and 3 mol/L) by hydrothermal method at 200 °C for 12 h: (a) $\delta = 0$ and (b) $\delta = 2$.

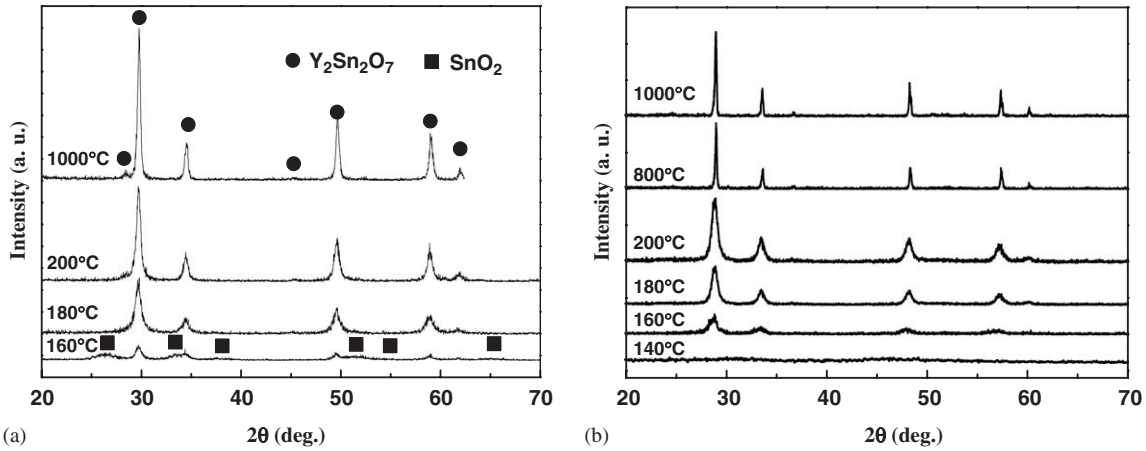

Fig. 2. The XRD patterns of (a) $Y_2Sn_2O_7$, and (b) $Bi_2Sn_2O_7$ synthesized under different temperatures by hydrothermal method and annealed at high temperature.

The above analysis sustains that the concentration of NaOH plays a critical role in the formation of phase-pure $Y_{2-\delta}Bi_\delta Sn_2O_7$ ($\delta = 0$, 0.1, 0.3, 0.5, 1.0, 1.5, and 2.0) by hydrothermal method. Only when the concentration of NaOH was 1 mol/L, the diffraction lines of the products can be indexed to a single-phase $Y_{2-\delta}Bi_\delta Sn_2O_7$. In order to synthesize phase-pure $Y_{2-\delta}Bi_\delta Sn_2O_7$ with different composition at same conditions, the nominal NaOH concentration of 1.0 M was chosen as an optimum concentration.

Fig. 2a shows the XRD patterns for the samples $Y_2Sn_2O_7$ synthesized under different temperatures (160, 180, and 200 °C) and the sample annealed at (1000 °C) for 8 h after hydrothermal method. We can see that when the synthetic temperature was 160 °C the products were the mixtures of SnO_2 and $Y_2Sn_2O_7$. When the temperature was increased to 180 °C phase-pure yttrium tin pyrochlore ($Y_2Sn_2O_7$) crystals were obtained. In order to identify the cubic pyrochlore phase of the samples synthesized by hydrothermal method did not change when it were annealed at high temperature, the samples were annealed at 1000 °C for 8 h after hydrothermal method. From Fig. 2a, we noted that only the peak intensity was enhanced with the increase of temperature while the peak position kept constant.

Fig. 2b shows the XRD for the samples ($\delta = 2$) synthesized under different temperatures (140, 160, 180, and 200 °C) by hydrothermal method and the XRD for the samples annealed at (800 and 1000 °C) for 8 h after hydrothermal method. From Fig. 2b, we can see that when the temperature was 140 °C the products were amorphous. With the increase of temperature, when the temperature was above the 160 °C phase-pure $Y_{2-\delta}Bi_\delta Sn_2O_7$ ($\delta = 2.0$) crystals were obtained. With the further increase of temperature, the peak intensity was enhanced while the peak position kept constant, which illustrated that the crystal size grew large with the increase of the temperature. Moreover, about the structure of $Bi_2Sn_2O_7$, there were some reports, it only adopts the regular pyrochlore structure at high temperatures while it appears tetragonal at room temperature with $a = \sqrt{2}a' = 15.01$ and $c = 2a' = 21.5$, where a' is the size of the cubic pyrochlore [10]. In our experiments, the cubic phase of the samples synthesized by hydrothermal method did not change when it were annealed at high temperature (800 and 1000 °C).

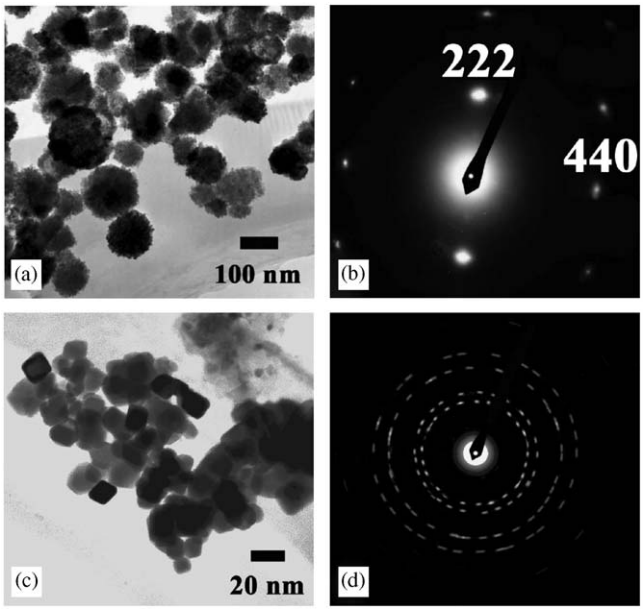

Fig. 3. The TEM micrographs and SAED patterns of $Y_2Sn_2O_7$ (a, b) and $Bi_2Sn_2O_7$ (c, d) powders synthesized by hydrothermal method at 200 °C.

Fig. 3 shows the TEM micrographs and SAED patterns of $Y_2Sn_2O_7$ (a, b) and $Bi_2Sn_2O_7$ (c, d) powders synthesized by hydrothermal method at 200 °C. As can be seen from Fig. 3a, the synthesized $Y_2Sn_2O_7$ powders had nearly spherical shape with rough surfaces and about 80 nm in diameter. Fig. 3b shows the SAED pattern taken from an individual $Y_2Sn_2O_7$ nanocrystal which shows that the

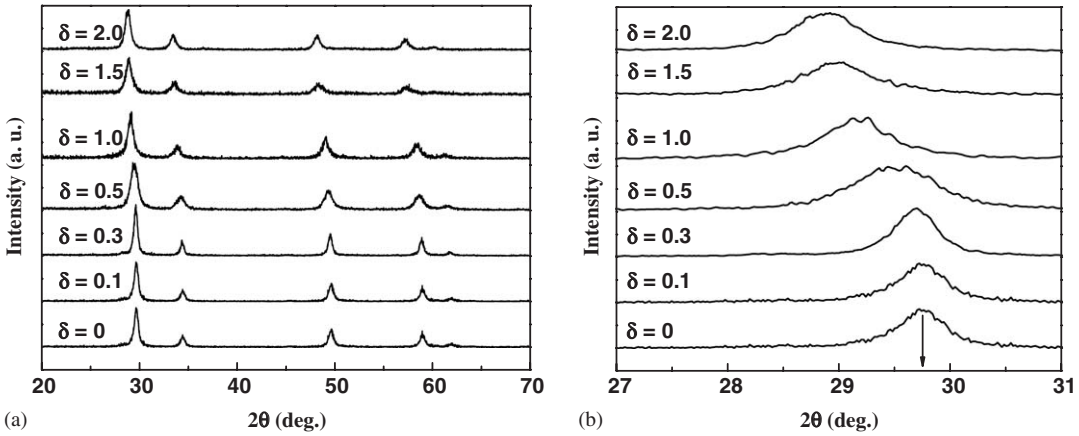

Fig. 4. The XRD of $Y_{2-\delta}Bi_{\delta}Sn_2O_7$ ($\delta = 0$, 0.1, 0.3, 0.5, 1.0, 1.5, and 2.0) synthesized by hydrothermal method at 200 °C for 12 h: (a) extended 2θ range; (b) zoomed 2θ range (27–31°).

nanoparticle was a single crystal of cubic $Y_2Sn_2O_7$. Fig. 3c reveals that the synthesized $Bi_2Sn_2O_7$ powders had nearly cubic shape with about 20 nm in diameter. The SAED pattern (d) is composed of many concentric circles which indicate the $Bi_2Sn_2O_7$ powders are composed of many small crystals of $Bi_2Sn_2O_7$.

The XRD patterns of $Y_{2-\delta}Bi_{\delta}Sn_2O_7$ ($\delta = 0$, 0.1, 0.3, 0.5, 1.0, 1.5, and 2.0) synthesized by hydrothermal method is shown in Fig. 4: (a) extended 2θ range; (b) zoomed 2θ range (27–31°). We note that all the diffraction peaks can be indexed to the pyrochlore structure without any impurity phase. With the increase of δ from 0 to 2.0, the obvious peak shift can be observed while the pure cubic phase has not been changed. All diffraction lines in the Fig. 4 ($\delta = 2$) can be readily indexed to a pure-phase $Bi_2Sn_2O_7$ with cubic lattice structure conforming to the *Fd3m* space group (JCPDS 17-0457).

The structural and thermal parameters for the $Y_{2-\delta}Bi_{\delta}Sn_2O_7$ at room temperature were determined by TOPAS program, which is a graphics-based profile analysis program built around a general non-linear least-squares fitting system. Being a linear combination of a Cauchyian and Gaussian functions, the pV function was selected which was the most reliable peak-shape function and was being widely used in the structure refinement software. The process of successive profile refinements modulated different structural and microstructural parameters of the simulated pattern to fit the experimental diffraction pattern. Profile refinement continues until convergence is reached in each case, with the value of the quality factor ($GoF = R_{wp}/R_{exp}$) approaching close to 1. The structural parameter and thermal parameters for the $Y_{2-\delta}Bi_{\delta}Sn_2O_7$ at room temperature are shown in Table 1. The results show that the lattice parameter a (Å) increases with the replacement of more yttrium atoms by bismuth atoms in the serials composition of $Y_{2-\delta}Bi_{\delta}Sn_2O_7$.

Fig. 5 shows the variation of the lattice parameter with the composition of the $Y_{2-\delta}Bi_{\delta}Sn_2O_7$. From Fig. 5, we noted that a continuous change in the lattice parameter

Table 1
The structural parameter and thermal parameters for the $Y_{2-\delta}Bi_{\delta}Sn_2O_7$ at room temperature

δ	a (Å)	R_p	R_{wp}	R_{exp}	GoF
0	10.374	1.83	2.51	9.95	0.25
0.1	10.409	1.11	1.58	5.21	0.30
0.3	10.418	3.49	4.57	13.13	0.35
0.5	10.484	2.16	2.95	10.45	0.28
1.0	10.569	5.05	6.38	9.10	0.70
1.5	10.660	2.72	3.44	10.43	0.33
2.0	10.703	4.86	6.08	9.35	0.65

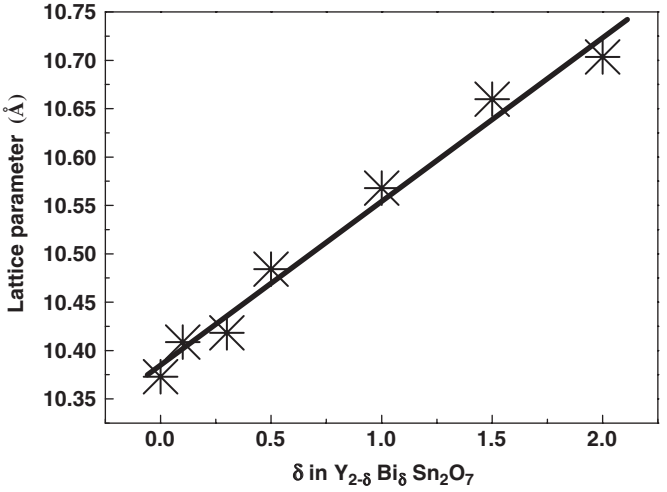

Fig. 5. Variation of the lattice parameter as a function of composition for the samples $Y_{2-\delta}Bi_{\delta}Sn_2O_7$ as determined from X-ray diffraction data.

versus composition, which is consistent with the Vegards's law, i.e. unit cell parameters change linearly with the composition [12]. This proves that the solid solutions are mutually miscible.

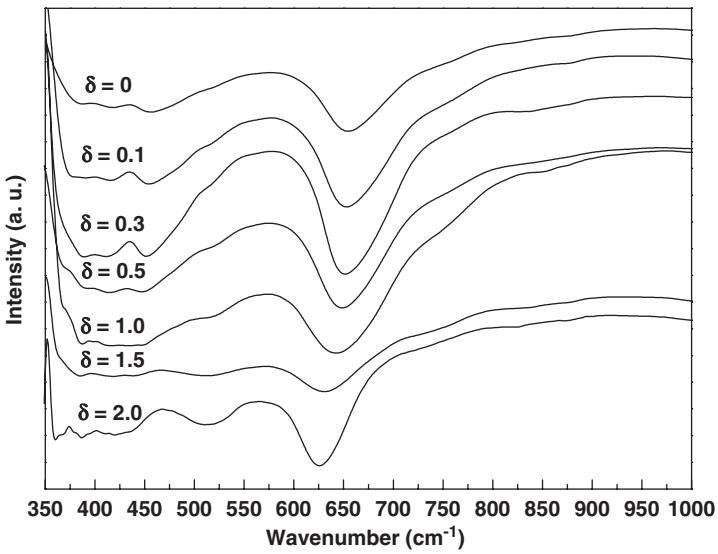

Fig. 6. IR spectra of compositions $Y_{2-\delta}Bi_{\delta}Sn_2O_7$ for various δ values.

It is noted that we report a synthesis method, based on a hydrothermal process, which is able to obtain a compound with any ratio of Y into the Bi site. The result is original because up to now the solubility limit was found to be $\delta = 1$ at 1000 °C [10]. Our preparation conditions eliminate the limit of the solid solution. The higher chemical homogeneity is probably responsible for our success. When the starting materials were dissolved in deionized water, the various ions formed an extensive mixture which decreases the ions diffuse distance that occurs in the crystallizing course. However, during the course of the solid reaction, the diffusion of ions between different microcrystals only obviously occurred at high temperature. Therefore, the crystallizing temperature was decreased in the hydrothermal condition.

The infrared (IR) absorption spectroscopy can be used to characterize the compound. The IR lattice vibration frequencies of some pyrochlore compounds with a formula $A_2B_2O_7$ have been studied. The IR absorption bands of solids in the range 100–1000 cm^{-1} are usually assigned to vibrations of ions in the crystal lattice [13]. There are seven IR-active optic modes originating from vibration and bending metal–oxygen bonds in the IR spectra of the pyrochlore oxides [9]. The band (v_1) at about 600 cm^{-1} is from the B–O stretching vibration in the BO_6 octahedron and the band (v_2) at about 500 cm^{-1} is from the A–O′ stretching vibration. In our IR spectra experiments, the spectra only in the region 350–4000 cm^{-1} are recorded. Only one broad band ascribable to B–O-stretching vibration was obviously observed for each sample. The IR spectra of the investigated $Y_{2-\delta}Bi_{\delta}Sn_2O_7$ with various δ values recorded in the range 350–1000 cm^{-1} are shown in Fig. 6 and the absorption bands are listed in Table 2. The difference between this work and that of Ref. [9] may result from the different preparation conditions. We notice a regularly shift of v (Sn–O) to low frequency with the replacement of smaller ion (Y^{3+}) by larger ones (Bi^{3+}) at the A-site in the series of $Y_{2-\delta}Bi_{\delta}Sn_2O_7$.

Table 2
The Sn–O stretching vibration IR band of the investigated $Y_{2-\delta}Bi_{\delta}Sn_2O_7$ with various δ values at room temperature

δ	0	0.1	0.3	0.5	1	1.5	2
v (B–O)	655	653	651	647	641	630	626

The relation between the frequency (in cm^{-1}) of the Sn–O vibration IR band, v (Sn–O), and the lattice parameter of the serials composition $Y_{2-\delta}Bi_{\delta}Sn_2O_7$ ($\delta = 0$, 0.1, 0.3, 0.5, 1.0, 1.5, 2.0) was shown in Fig. 7. The v (Sn–O) value decreased almost linearly with the increasing of lattice constant a or δ, indicating that the Sn–O bond strength weakens with the increase of lattice constant a or δ. This similar linear relationship between the frequency of the Sn–O vibration and the A-ion radius with constant B-ion radius in rare-earth stannate pyrochlores has been described by Teraoka et al. [5]. The change in the Sn–O bond strength might be ascribable to that of the bond distance, because the Sn–O bond distance of rare-earth stannate pyrochlores is reported to increase monotonically with increasing a or r_A [14]. In the serials composition $Y_{2-\delta}Bi_{\delta}Sn_2O_7$, the volume increasing associated with the replacement of smaller ion (Y^{3+}) by larger ion (Bi^{3+}) at the A-site has appreciable influence on the bonding character of Sn–O bonds. The frequency of the B–O vibration was mainly affected by the A-ion radius with constant B-ion radius in stannate pyrochlores. The larger the A-ion radius (with the same B-ion) the lower the observed B–O vibrational frequency, indicating that the force constant has decreased.

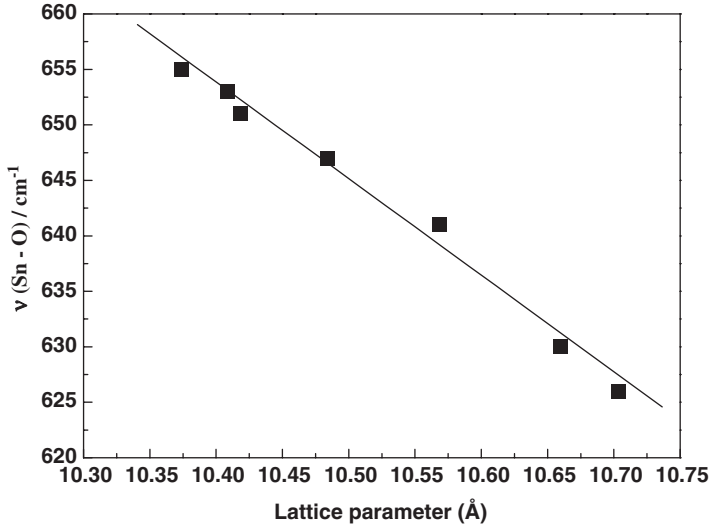

Fig. 7. Relation between the frequency (in cm^{-1}) of the Sn–O vibration IR band, v (Sn–O), and the lattice parameter of stannate pyrochlores.

4. Conclusions

In this paper, we report a synthesis method based on a hydrothermal process, which is able to obtain a series of $Y_{2-\delta}Bi_{\delta}Sn_2O_7$ ($\delta = 0$, 0.1, 0.3, 0.5, 1.0, 1.5, and 2.0) nanocrystals with any ratio of Y into a Bi site at low temperature of 200 °C. The higher chemical homogeneity is probably responsible for our success. The characterization of TEM and SAED of samples revealed that $Y_2Sn_2O_7$ and $Bi_2Sn_2O_7$ had nearly 80 nm diameters spherical single crystals with rough surfaces and about 20 nm diameters small crystals with cubic shape, respectively. In addition, we notice a continued change in the lattice parameter versus composition, which is consistent with the Vegards's law. IR spectra of compounds $Y_{2-\delta}Bi_{\delta}Sn_2O_7$ revealed the v (Sn–O) value decreased almost linearly with the increasing of lattice constant a or δ. The successful synthesis of serial $Y_{2-\delta}Bi_{\delta}Sn_2O_7$ indicates that the chemical synthesis conferred a higher chemical homogeneity and reactivity on the powders, and resulting in low crystallization temperature for the pyrochlore-phase complex oxides.

References

[1] B. Mazumder, J.C. Vedrine, Appl. Catal. A: Gen. 245 (2003) 87–102.
[2] T. Mallat, Z. Bodnar, P. Hug, A. Bailker, J. Catal. 153 (1995) 131–143.
[3] M. Besson, F. Lahmer, P. Gallezot, P. Fuertes, G. Fleche, J. Catal. 152 (1995) 116–121.
[4] L. Moensa, P. Ruizb, B. Delmonb, D. Devillers, Appl. Catal. A: Gen. 180 (1999) 299–315.
[5] Y. Teraoka, K.I. Torigoshi, H. Yamaguchi, T. Ikeda, S. Kagawa, J. Mol. Catal. A: Chem. 155 (2000) 73–80.
[6] A.M. Srivastava, Mater. Res. Bull. 37 (2002) 745–751.
[7] V. Ravi, S. Adyanthaya, M. Aslam, S. Pethkar, V.D. Choube, Mater. Lett. 40 (1999) 11–13.
[8] Z.G. Lu, J.W. Wang, Y.G. Tang, Y.D. Li, J. Solid State Chem. 177 (2004) 3075–3079.
[9] M.A. Subramanian, G. Aravamudan, G.V. Subba Rao, Prog. Solid State Chem. 15 (1983) 55–143.
[10] Ismunandar, B.J. Kennedy, B.A. Hunter, T. Vogt, J. Solid State Chem. 131 (1997) 317–325.
[11] S.M. Zanetti, S.A. da Silva, G.P. Thim, J. Solid State Chem. 177 (2004) 4546–4551.
[12] A.R. West, Solid State Chemistry and Its Applications, Wiley, New Delhi, 1988.
[13] M.T. Vandenborre, E. Husson, J.P. Chatry, D. Michel, J. Raman Spectrosc. 14 (1983) 63–71.
[14] B.J. Kennedy, B.A. Hunter, C.J. Howard, J. Solid State Chem. 130 (1997) 58–65.